AIAA JOURNAL
Vol. 39, No. 1, January 2001

Hybrid Aeroelastic Optimization and Antioptimization

Massimiliano Zingales* and Isaac Elishakoff†
Florida Atlantic University, Boca Raton, Florida 33431-0991

A simple aeroelastic structure possessing uncertain elastic modulus, which is modeled as varying either in a convex hull of experimental data points or within an approximating ellipse of minimum area containing all of the data, is studied. A solution of an antioptimization problem, which is defined as the search for the worst critical velocity under uncertainty constraint is determined. At the second stage, the optimization problem is addressed as an evaluation of the design variables, such that the worst critical velocity is made to exceed a preselected velocity. It appears that, due to the unavoidable presence of uncertainties, realistic aeroelastic problems ought to be posed as a hybrid optimization and as antioptimization procedures. Several numerical results are elucidated to illustrate the ideas.

I. Introduction

THE notion of antioptimization of structures was introduced by Elishakoff.[1,2] Since then, it has been applied to the design of structures with bounded, both nonprobabilistic and nonfuzzy uncertainty, by several authors. The reader can consult with studies by Elishakoff et al.,[3] Adali et al.,[4] and Haftka and Lombardi.[5] In this paper we apply the hybrid optimization and antioptimization to aeroelastic problems.

Optimization of structures with aeroelastic constraints has been dealt with by several authors. A partial list of works includes those by Turner,[6] Plaut,[7] Ashley,[8] Librescu and Bainer,[9] Shirk et al.,[10] Ringertz,[11] Livne and Mineau,[12] Pierson and Genalo,[13] and Bishop et al.[14] However, the uncertainty in elastic moduli or in the material properties in conjunction with the aeroelastic optimization is a relatively new topic. It has been addressed in the probabilistic setting by Kuttekueler and Ringertz.[15] The stochastic finite element method for reliability of plates in supersonic flow was introduced by Liaw and Yang.[16] In the future, one would anticipate an increased utilization of the stochastic finite element method in conjunction with aeroelastic phenomena. In this respect it is instructive to quote Shinozuka[17]:

> . . . it is recognized that it is rather difficult to estimate experimentally the auto-correlation function, or in the case of weak homogeneity, the spectral density function of the stochastic variation of material properties. In view of this, the upper bound results are particularly important, since the bounds derived . . . do not require knowledge of the auto-correlation function.

This observation may limit the applicability of probabilistic analysis to uncertainty. In these circumstances one should look for alternatives to the notion of stochasticity. As Livne[18] mentions in his careful overview of the subject of aeroelastic optimization,

> . . .approaches for addressing uncertainty in design optimization of structural systems are still in various stages of study and evaluation. . . Ranging from statistical methods, in which the statistical characteristics of uncertainties are known or assumed, or methods based on fuzzy logic, as well as methods which use bounds on the system uncertainties to optimize for a worst case combination of pre-assigned parameter and modeling errors—all these methods have not been compared yet in the context of aeroelasticity and areoservoelasticity of fixed wing airplanes.

In this study we adopt an antioptimization analysis that utilizes information that is easier to obtain (than either a stochasticity- or fuzzy-sets-based approach), namely, the region of variation of the elastic moduli.[19] Because of this partial information, it is sensible to require only the fragmentary characterization of the response: namely, the determination of the maximum and minimum values of the critical velocity. Once the minimum of the velocity is determined, the structural parameters are chosen so as to exceed some preselected velocity. Numerous examples are elucidated to gain physical insights into the problem.

Received 30 December 1998; revision received 27 October 1999; accepted for publication 27 October 1999.

*Research Assistant, Department of Mechanical Engineering.
†Professor, Department of Mechanical Engineering.

II. Deterministic Theoretical Analysis

Let us consider a Bernoulli–Euler's beam with variable cross section and nonhomogenous elastic properties; the beam is subjected to a supersonic stream flow in the x direction.

The Young's modulus of the beam $E(x)$ is represented by the following expression:

$$E(x) = \varphi_1(x)E_1 + \varphi_2(x)E_2 \tag{1}$$

where E_1 and E_2 can be characterized as amplitudes and $\varphi_1(x)$ and $\varphi_2(x)$ are continuous nondimensional functions governing the variation of the modulus $E(x)$. In this section, we abstain from specifying particular forms of the functions $\varphi_1(x)$ and $\varphi_2(x)$, except noting that they should be chosen to satisfy the obvious physical requirement $E(x) > 0$. The beam's width $b(x)$ and its thickness $h(x)$ are considered as varying along the abscissa x:

$$b(x) = b_0\chi_b(x),\ h(x) = h_0\chi_h(x) \tag{2}$$

where b_0 and h_0 are positive constants and $\chi_b(x)$ and $\chi_h(x)$ are shape functions governing the variation of the beam's width $b(x)$ and depth $h(x)$, respectively. Moreover, χ_b and χ_h equal unity at the coordinate origin $\chi_b(0) = \chi_h(0) = 1$. Therefore, b_0 and h_0 represent the width and the depth of the cross section at $x = 0$. The description of the aeroelastic interaction between the beam's transverse deflection $w(x, t)$ and the air pressure load will be performed by means of the piston theory.[20–22] The effect of the structural and aerodynamic dampings on the beam's behavior $w(x, t)$ will be excluded for the sake of simplicity. The equation of motion reads

$$\frac{\partial^2}{\partial x^2}\left(E(x)I(x)\frac{\partial^2 w(x,t)}{\partial x^2}\right) + \rho A(x)\frac{\partial^2 w(x,t)}{\partial t^2} + \frac{kp_\infty}{c_\infty}\left(U\frac{\partial w}{\partial x}\right) = 0 \tag{3}$$

where $A(x)$ is the cross-sectional area, $I(x)$ the moment of inertia, and ρ the structural mass density. The gas-flow interaction is represented by the last term in Eq. (3), where k is the exponent of the polytropic thermodynamic transformation, p_∞ is the pressure of the nondisturbed gas flow, c_∞ is the speed of the shock waves in the nonperturbed airstream, and U is the motion relative velocity between the gas flow and the system. The boundary conditions associated with the simply supported beam read

$$w(x,t) = \frac{\partial^2 w}{\partial x^2} = 0, \qquad \text{at} \qquad x = 0 \tag{4a}$$

$$w(x,t) = \frac{\partial^2 w}{\partial x^2} = 0, \qquad \text{at} \qquad x = L \tag{4b}$$

where L is the beam's length. The initial conditions are

$$w(x,0) = \frac{\partial w(x,t)}{\partial t} = 0, \qquad \text{at} \qquad t = 0 \tag{5}$$

The governing equation for the beam's deflection $w(x,t)$ is not solvable exactly for arbitrary choice of the functions $\varphi_1(x)$, $\varphi_2(x)$, $\chi_b(x)$, and $\chi_h(x)$. Hereinafter, the Bubnov–Galerkin's approach will be utilized. We approximate the solution as follows:

$$w(x,t) = \sum_{i=1}^{N} \psi_i(x) f_i(t) \tag{6}$$

with N denoting the number of retained terms in the expansion and $\psi_i(w)$ designating known comparison functions satisfying all boundary conditions in Eq. (4). We substitute Eq. (6) into Eq. (3) and require that the inner product vanishes:

$$(\varepsilon, \psi_j) = 0 \qquad (j = 1, 2, \ldots, N) \tag{7}$$

where

$$(\varepsilon, \psi_j) = \int_0^L \varepsilon(x)\psi_j(x)\,\mathrm{d}x \tag{8}$$

This procedure leaves us with a set of ordinary differential equations:

$$\sum_{\alpha=1}^{N} K_{\alpha\beta} f_\alpha(t) + \sum_{\alpha=1}^{N} M_{\alpha\beta} \ddot{f}_\alpha(t) + U \frac{kp_\infty}{c_\infty} \sum_{\alpha=1}^{N} N_{\alpha\beta} f_\alpha(t) = 0$$

$$(\beta = 1, 2, \ldots, N) \tag{9}$$

The coefficients appearing in Eq. (9) are given as follows:

$$K_{\alpha\beta} = \int_0^L \psi_j(x) \frac{\mathrm{d}^2}{\mathrm{d}x^2}\left(E(x)I(x)\frac{\mathrm{d}^2\psi_\alpha(x)}{\mathrm{d}x^2}\right)\mathrm{d}x$$

$$M_{\alpha\beta} = \int_0^L \rho A(x)\psi_\alpha(x)\psi_\beta(x)\,\mathrm{d}x$$

$$N_{\alpha\beta} = \frac{kp_\infty}{c_\infty} \int_0^L \frac{\mathrm{d}\psi_\alpha(x)}{\mathrm{d}x}\psi_\beta(x)\,\mathrm{d}x \tag{10}$$

The solution of the system in Eq. (9) is furnished in the form

$$f_\alpha(t) = A_\alpha e^{i\omega t} \qquad (\alpha = 1, 2, \ldots, N) \tag{11}$$

where ω represents the sought eigenvalue. We arrive at an algebraic homogeneous system of the equations for A_α:

$$\sum_{\alpha=1}^{N} K_{\alpha\beta} A_\alpha - \sum_{\alpha=1}^{N} \omega^2 M_{\alpha\beta} A_\alpha + U \sum_{\alpha=1}^{N} N_{\alpha\beta} A_\alpha = 0$$

$$(\beta = 1, 2, \ldots, N) \tag{12}$$

To obtain a the nontrivial solution, namely,

$$\sum A_j^2 \neq 0$$

one requires the determinant of the coefficient matrix of the system in Eq. (12) to vanish:

$$\det\left[-\omega^2 M_{\alpha\beta} + U N_{\alpha\beta} + K_{\alpha\beta}\right] = 0 \tag{13}$$

leading to the approximate eigenfrequency equation for ω.

III. Stability Analysis Within Two-Term Approximation

Let us confine our analysis to the case with only two terms retained in Eq. (6). In this case the system in Eq. (12) is reduced to the two equations

$$A_1\left(K_{11} - \omega^2 M_{11} + U^* N_{11}\right) + A_2\left(K_{12} - \omega^2 M_{12} + U^* N_{12}\right) = 0$$

$$A_1\left(K_{21} - \omega^2 M_{21} + U^* N_{21}\right) + A_2\left(K_{22} - \omega^2 M_{22} + U^* N_{22}\right) = 0 \tag{14}$$

It is instructive to cast Eq. (14) in terms of the natural frequencies of the system $\bar{\omega}_1^2$ and $\bar{\omega}_2^2$. First, as an auxiliary problem, consider the free-vibration case

$$\det\left[-\bar{\omega}^2 M_{\alpha\beta} + K_{\alpha\beta}\right] = 0 \qquad (\alpha, \beta = 1, 2) \tag{15}$$

resulting in the biquadratic

$$\bar{\omega}^4 - c_1\bar{\omega}^2 + c_2 = 0 \tag{16}$$

with the coefficients given by

$$c_1 = \frac{K_{11}M_{22} + K_{22}M_{11} - K_{12}M_{21} - K_{21}M_{12}}{\det[M_{\alpha\beta}]}$$

$$c_2 = \frac{\det[K_{\alpha\beta}]}{\det[M_{\alpha\beta}]} \tag{17}$$

whose solutions

$$\bar{\omega}_1^2 = \left(c_1 - \sqrt{c_1^2 - 4c_2}\right)\Big/2, \qquad \bar{\omega}_2^2 = \left(c_1 + \sqrt{c_1^2 - 4c_2}\right)\Big/2 \tag{18}$$

represent the natural frequencies of vibration.[23] Because of Vieta's theorem, $c_1 = -(\bar{\omega}_1^2 + \bar{\omega}_2^2)$ and $c_2 = \bar{\omega}_1^2\bar{\omega}_2^2$. Hence, Eq. (13) can be rewritten in the following form:

$$\omega^4 + \left[\left(\bar{\omega}_1^2 + \bar{\omega}_2^2\right) + d_1 U^*\right]\omega^2 + \bar{\omega}_1\bar{\omega}_2 + d_2 U^* + d_3 (U^*)^2 = 0 \tag{19}$$

with terms d_i defined as

$$d_1 = \frac{N_{11}M_{22} + N_{22}M_{11} - N_{12}M_{21} - N_{21}M_{12}}{\det[M_{\alpha\beta}]}$$

$$d_2 = \frac{K_{11}N_{22} + K_{22}N_{11} - K_{12}N_{21} - K_{21}N_{12}}{\det[M_{\alpha\beta}]}$$

$$d_3 = \frac{\det[N_{\alpha\beta}]}{\det[M_{\alpha\beta}]} \tag{20}$$

Equation (11) suggests that once the frequency ω takes complex values, the dynamic instability flutter occurs. The critical condition appears when the discriminant D

$$D = \left[U^* d_1 + \left(\bar{\omega}_1^2 + \bar{\omega}_2^2\right)\right]^2 - 4\left[\bar{\omega}_1^2\bar{\omega}_2^2 + U^* d_2 + (U^*)^2 d_3\right] \tag{21}$$

of the biquadratic Eq. (19) vanishes, yielding the flutter velocity

$$U_{\mathrm{cr}} = \left(d_1^2 - 4d_3\right)^{-1}\left\{d_1^2\left(\bar{\omega}_1^2 + \bar{\omega}_2^2\right) + 2d_2 + \sqrt{\left[d_1^2\left(\bar{\omega}_1^2 + \bar{\omega}_2^2\right) + 2d_2\right]^2 - \left(\bar{\omega}_1^2 - \bar{\omega}_2^2\right)^2\left(d_1^2 - 4d_3\right)}\right\} \tag{22}$$

For values larger than U_{cr}, the discriminant takes a negative sign, and the roots are complex conjugate. For the case of the beam simply supported at both ends, the following set can be utilized for the comparison functions:

$$\psi_\alpha(x) = \sin(\alpha\pi x/L) \tag{23}$$

which represent the exact mode shapes of the associated uniform beam. Note that in these circumstances,

$$N_{11} = N_{22} = 0, \qquad N_{12} = -N_{21} \tag{24}$$

yielding

$$U_{\rm cr} = \frac{\bar{\omega}_2^2 - \bar{\omega}_1^2}{2\sqrt{d_3}} = \frac{\left(\bar{\omega}_2^2 - \bar{\omega}_1^2\right)\sqrt{\det[M_{\alpha\beta}]}}{2N_{12}} \tag{25}$$

Observe that Eq. (25) formally coincides with expression (4.104) by Bolotin[22] for the uniform beam. The difference lies in the definition of the natural frequencies $\bar{\omega}_\alpha$.

Recall that E_1 and E_2 are uncertain variables, leading to variability of the flutter velocity. The following question arises: How should one take into account the variability of the elastic moduli on $U_{\rm cr}$?

IV. Convex Modeling of Uncertain Moduli

In this section the uncertainty in the Young's modulus $E(x)$, represented in Eq. (1), will be specified. In many recent investigations the elastic modulus is treated as the random field, and the problems are solved by the finite element method necessitating the knowledge of the autocorrelation function of the elasticity modulus. Often, however, such information is unavailable. In these circumstances one can act in one of the following ways: Either postulate that such an autocorrelation function is known, or pick up (as is usually done), any allowable autocorrelation function based on the assumption that once the autocorrelation function will become available, it could be introduced into the analysis. Another way will be to abandon this excessively demanding analysis and look for an approach that does not postulate that uncertainty and probability are synonymous.

In this study we use a nonprobabilistic model of uncertainty. The two amplitude parameters E_1 and E_2 are treated as uncertain variables, varying in a convex domain C. The admissible region of variation R (Fig. 1) is then described by an inequality:

$$(E_1, E_2) \in C \tag{26}$$

The domain C for E_1 and E_2 will be assumed to lie entirely in the positive quadrant of the plane E_1, E_2. Because of the variability of $U_{\rm cr}$, it appears natural to evaluate the worst critical velocity $U_{\rm cr,worst}$, when E_1 and E_2 vary in C. This is somewhat opposite to usual engineering practice of looking for the best solutions. To underline this contrast, the methodology of looking for the worst solution was dubbed by Elishakoff[1] an antioptimization process. Thus, we are looking for

$$U_{\rm cr,worst} = \min_{(E_1,E_2)\in C} U_{\rm cr}(E_1, E_2) \tag{27}$$

Note that the coefficient c_1 in Eq. (18) is a linear function of E_j $(j = 1, 2)$, whereas the coefficient c_2 is a quadratic function of them, that is,

$$c_1 = \delta_1 E_1 + \delta_2 E_2, \qquad c_2 = \varepsilon_{11}E_1^2 + \varepsilon_{12}E_1E_2 + \varepsilon_{22}E_2^2 \tag{28}$$

where

$$\begin{aligned}
\delta_1 &= (M_{22}K_{111} + M_{11}K_{221} - M_{12}K_{211} - M_{21}K_{121}) \\
\delta_2 &= (M_{22}K_{112} + M_{11}K_{222} - M_{12}K_{212} - M_{21}K_{122}) \\
\varepsilon_{11} &= K_{111}K_{221} - K_{121}K_{221}, \qquad \varepsilon_{22} = K_{112}K_{222} - K_{122}K_{212} \\
\varepsilon_{12} &= K_{111}K_{222} + K_{112}K_{221} - K_{121}K_{212} - K_{122}K_{211}
\end{aligned} \tag{29}$$

The expression for K_{ijl} reads

$$K_{ijl} = \int_0^L \psi_j(x) \frac{\mathrm{d}^2}{\mathrm{d}x^2}\left(I(x)\varphi_l(x)\frac{\mathrm{d}^2\psi_i(x)}{\mathrm{d}x^2}\right)\mathrm{d}x \tag{30}$$

Bearing in mind Eqs. (25) and (26), we can rewrite Eq. (25) for the critical velocity squared as follows:

$$U_{\rm cr}^2(E_1, E_2) = d_{11}E_1^2 + 2d_{12}E_1E_2 + d_{22}E_2^2 \tag{31}$$

where

$$d_{11} = \frac{\delta_1^2 \det[M_{\alpha\beta}] - 4\varepsilon_{11}}{\left\{4N_{12}^2\det[M_{\alpha\beta}]\right\}}, \qquad d_{12} = \frac{2\delta_1\delta_2/\det[M_{\alpha\beta}] - 4\varepsilon_{12}}{\left\{8N_{12}^2\det[M_{\alpha\beta}]\right\}}$$

$$d_{22} = \frac{\delta_2^2 \det[M_{\alpha\beta}] - 4\varepsilon_{22}}{\left\{4N_{12}^2\det[M_{\alpha\beta}]\right\}} \tag{32}$$

One recognizes that the expression of the critical velocity is a quadratic form in variables E_1 and E_2. In matrix form, Eq. (31) can be rearranged as

$$U_{\rm cr}^2 = E^T D E \tag{33}$$

with

$$E^T = [E_1 \quad E_2], \qquad D = \begin{pmatrix} d_{11} & d_{12} \\ d_{12} & d_{22} \end{pmatrix} \tag{34}$$

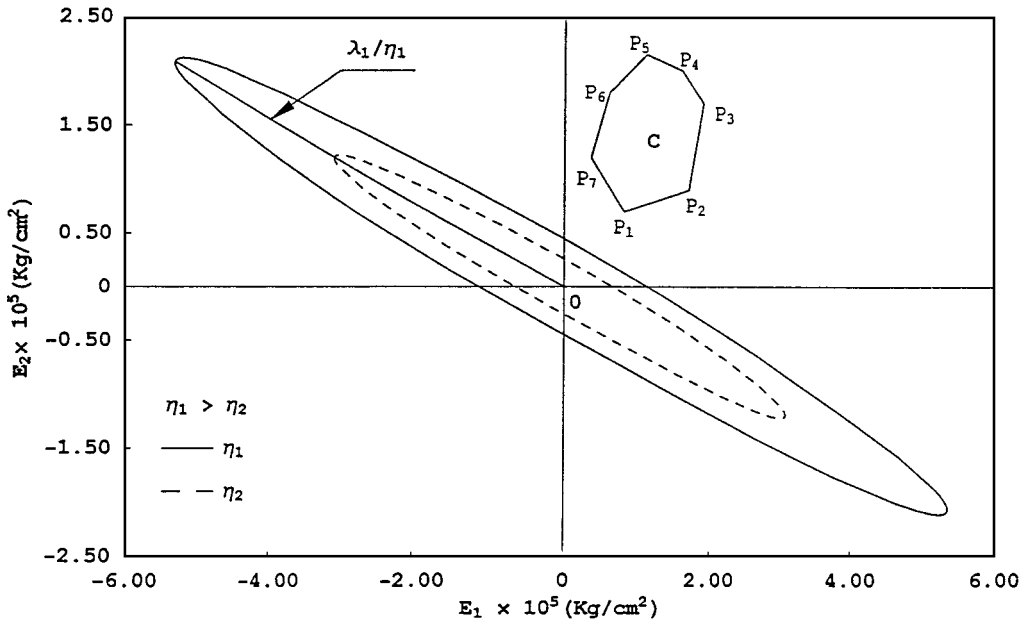

Fig. 1 Shape and location of the uncertainty region and of the η^2 ellipses.

Accounting for the physical meaning of the right-hand side in Eq. (30), we can conclude that the matrix D is positive definite. Therefore, Eq. (31), conveniently rewritten in the form

$$E^T DE - U_{\rm cr}^2 = 0 \tag{35}$$

represents an ellipse in the plane (E_1, E_2) with the center coinciding with the origin of the coordinate system. We thus obtain a family of homotetic ellipses corresponding to different values of $U_{\rm cr}^2$ if the latter is treated as an independent parameter. Naturally, the larger values of $U_{\rm cr}^2$ correspond to larger semi-axes of the ellipse in the plane. For small values of $U_{\rm cr}^2$ the ellipse in Eq. (31) and the region in Eq. (26) are disjoint. For large values of it they have a common area. Therefore, there exist two values of $U_{\rm cr}^2$, denoted $U_{\rm cr,worst}^2$ and $U_{\rm cr,best}^2$, respectively, with $U_{\rm cr,worst}^2 < U_{\rm cr,best}^2$, for which the two convex domains in Eqs. (26) and (31) share a single point. One of the values corresponds to the case when one ellipse contains the other one entirely, whereas the other point is associated with the case when they are on the different sides of the common tangent.

Values of $U_{\rm cr}^2$ falling outside of the interval $[U_{\rm cr,worst}^2, U_{\rm cr,best}^2]$ do not represent feasible critical velocities because the set (E_1, E_2) will not satisfy Eq. (26). Note that the two values of velocities, $U_{\rm cr,worst}^2$ and $U_{\rm cr,best}^2$, represent, respectively, the smallest and the largest solutions allowed by Eq. (26). To determine these values we need to examine closely the relative spacing of the critical velocity ellipse and the region of uncertain variation of the elastic moduli. According to the interpretation of the parameters E_1 and E_2 as some effective moduli of elasticity, we shall confine our analytical derivation to the arc of ellipse in Eq. (35) contained in the first quadrant of the plane (E_1, E_2). It can be shown (Appendix A) that, under some assumptions about the functions $\varphi_i(x)$, the critical velocity ellipse in Eq. (35) is always oriented with its major axis in the second and fourth quadrant of the plane (E_1, E_2), as in Fig. 1.

Once the orientation of the ellipse, representing the critical velocity $U_{\rm cr}^2$ with respect to region of variation C of the uncertain parameters E_1 and E_2 has been identified, one can solve analytically the antioptimization problem. The following sections will be concerned with the solution of the problem in Eq. (27) for various practical shapes of the uncertainty region.

Prior to proceeding further, let us pose the following question: Why do we need to consider various shapes of the uncertainty region? To reply to this question, we visualize that the results of the experimental measurements yield an ensemble of functions $E_i(x)$. These functions are then decomposed to sets of pairs (E_{1i}, E_{2i}). Each of these pairs forms a point in the plane (E_1, E_2). We then are interested in determining the region that contains all of these points. A convex hull of these points is naturally such a set, forming a polygonal uncertainty region. Also, it is easily visualized that different researchers and engineers may approximate the uncertainty region via differing means. It makes sense, therefore, to treat different possibilities.

V. Antioptimization Problem: Polygonal Region of Uncertainty

In this section we consider an uncertainty set C possessing a polygonal shape with m vertices. The vertices $P_i (i = 1, \ldots, m)$ of the polygon have coordinates $P_i = (E_{1i}, E_{2i})$, respectively. We denote the vertex in the lowest-left corner by P_1, the others are numbered counterclockwise as P_2, P_3, etc. (Fig. 1). Hereinafter we form a set V of distances d_i of the vertices from the origin O:

$$V = \{d_1, \ldots, d_m\}, \qquad d_i = \sqrt{E_{1,i}^2 + E_{2,i}^2} \tag{36}$$

As is established in Eq. (A1), the result of antioptimization is given by the joint points of the homotetically inflated ellipse in Eq. (31) and the convex uncertainty region C. The critical velocity in Eq. (32) depends on the values of the design variables b_0 and h_0, appearing in Eq. (2), in addition to uncertain variables E_1 and E_2. This dependence can be highlighted by rewriting Eq. (31) in the form

$$U_{\rm cr}^2 = b_0^2 h_0^6 \eta^2 \tag{37}$$

with the positive coefficient

$$\eta^2 = d_{11n} E_1^2 + 2 d_{12n} E_1 E_2 + d_{22n} E_2^2 \tag{38}$$

The coefficients $d_{ijn} (i, j = 1, 2)$ in Eq. (38) are obtained from Eq. (31) by formally letting $b_0 = h_0 = 1$. Because the critical velocity depends on the uncertain parameters of elasticity E_i through the coefficient η^2, the antioptimization problem will focus on the determination of the extrema of the coefficient η^2 provided that E_1 and E_2 vary in region C. Equation (38) represents a family of concentric ellipses in the plane E_1 and E_2 obtained by varying the value of the coefficient η^2. The major axis passes through in the second and fourth quadrants of the plane E_1 and E_2. As shown in Sec. IV for the critical velocity (and hence η^2), the ellipse in Eq. (38) and the region of uncertainty C must share a common point. There are two possibilities for such a point to exist. One, $P_{\rm best}$ corresponds to the maximum of η^2, whereas the minimum is associated with point $P_{\rm worst}$.

The extreme values of the coefficient η^2 are found by substituting the coordinates $E_{1,\rm worst}$, $E_{2,\rm worst}$ and $E_{1,\rm best}$, and $E_{2,\rm best}$ of the points P_w and P_b into Eq. (38). Bearing in mind Eq. (38), the expressions for the maximum and minimum value of the critical flutter velocity, denoted in the following, $U_{\rm cr,best}^2$ and $U_{\rm cr,worst}^2$ become

$$U_{\rm cr,best}^2 = b_0^2 h_0^6 \eta_{\max}^2 = b_0^2 h_0^6 \left(d_{11n} E_{1,b}^2 + 2 d_{12n} E_{1,b} E_{2,b} + d_{22n} E_{2,b}^2 \right) \tag{39}$$

$$U_{\rm cr,worst}^2 = b_0^2 h_0^6 \eta_{\min}^2 = b_0^2 h_0^6 \left(d_{11n} E_{1,w}^2 + 2 d_{12n} E_{1,w} E_{2,w} + d_{22n} E_{2,w}^2 \right) \tag{40}$$

The expression of the coordinates corresponding to the points $P_{\rm worst}$ and $P_{\rm best}$ are given in Appendix B for all the cases reported in Figs. 2a and 2b.

Comparing the ellipses in Fig. 1 with those in Fig. 2a, we observe that they possess different ratios of their respective semi-axes $e = \lambda_1 / \lambda_2$, referred to as eccentricity e. This is because the functions $\varphi_1(x)$ and $\varphi_2(x)$ chosen in Fig. 1 are $\varphi_1(x) = 1 + 5.3 \times (x/L)^2 + 0.5 \times (x/L)^3$ and $\varphi_2(x) = 1 + 2(x/L)$, whereas in Fig. 2a they read $\varphi_1(x) = 1 - 3(x/L)^2$ and $\varphi_2(x) = 0.001 + 0.3(x/L)$. The shape functions for Fig. 2 $\varphi_j(x)$ are positive in the interval $[0, L]$. The function $\varphi_1(x)$ chosen for Fig. 2a takes on negative values in the interval $[L\sqrt{3}/3, L]$. Still, the modulus of elasticity is a positive quantity. Despite the function $\varphi_1(x)$ not being positive in the whole entire interval $[0, L]$, the major axis of the η^2 ellipse lies in the second and fourth quadrants of the plane E_1 and E_2. Numerical calculations show that the positiveness requirement of functions $\varphi_1(x)$ and $\varphi_2(x)$ in the interval $[0, L]$ leads to a large eccentricity e of the η^2 ellipse. The weaker condition that $E(x)$ is positive but $\varphi_j(x)$ may not be results in lower values of the eccentricity e. The particular choice of the shape functions $\varphi_1(x)$ and $\varphi_2(x)$ in Fig. 2a has been made to enable an easier visualization of the ellipses corresponding to extremal values $\eta_{\min}^2$ and $\eta_{\max}^2$.

The objective of the next section is to drive approximations of the admissible region for E_1 and E_2 by a continuous, smooth curve for analytical purposes.

VI. Antioptimization of Flutter Velocity: Elliptical Region of Uncertainty

Let us assume that the region C is represented by an elliptical area with the abscissa and the ordinate of the center C_0 denoted by E_{10} and E_{20}, respectively:

$$(E_1 - E_{10})^2 \big| \, a^2 + (E_2 - E_{20})^2 \big| \, b^2 \le 1 \tag{41}$$

where a and b represent the semi-axes of the ellipse Figs. 3a and 3b. We are looking for the points $P_{\rm worst} \equiv (E_{1,w}, E_{2,w})$ and $P_{\rm best} \equiv (E_{1,b}, E_{2,b})$ that satisfy Eqs. (39) and (40) and correspond, respectively, to the worst and the best critical velocities $U_{\rm cr,worst}$ and $U_{\rm cr,best}$ given in Eq. (63). In the following, we denote the coordinates of the points $P_{\rm worst}$ and $P_{\rm best}$, respectively, as $\bar{e}_{1,\rm worst}$, $\bar{e}_{2,\rm worst}$, and $\bar{e}_{1,\rm best}$, $\bar{e}_{2,\rm best}$. The procedure to obtain the coordinate of the extrema of the critical velocity is illustrated in Appendix C. The values

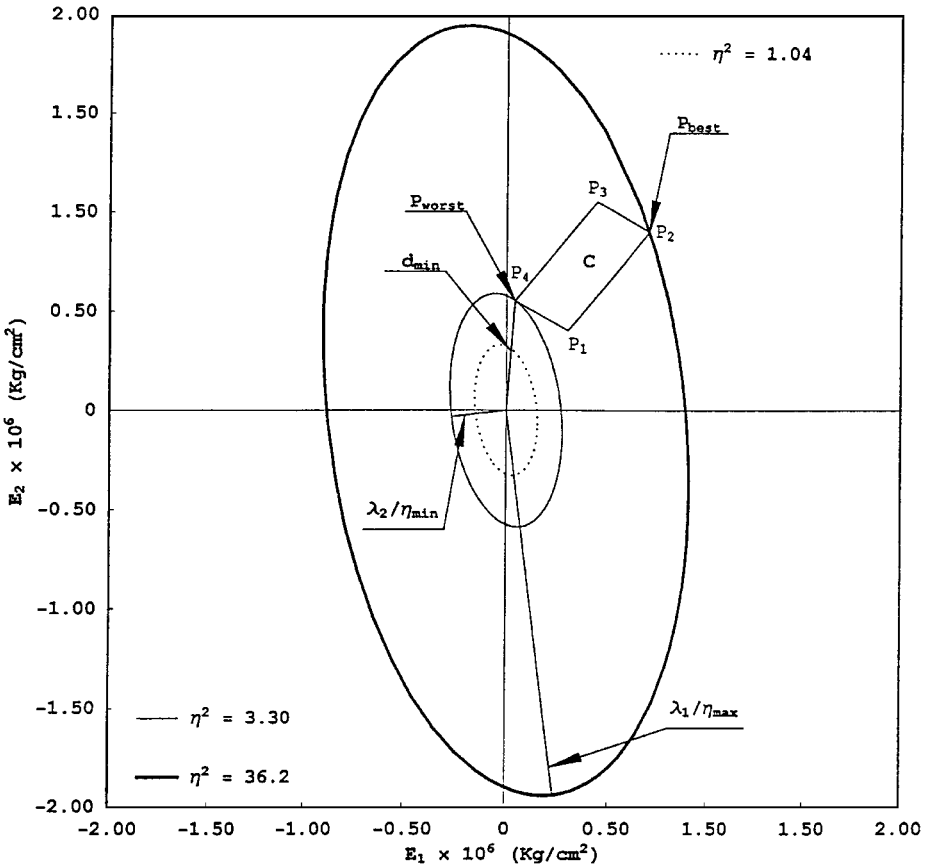

Fig. 2a Rectangular region of uncertainty, $\eta^2_{\max}$ and $\eta^2_{\min}$ ellipses.

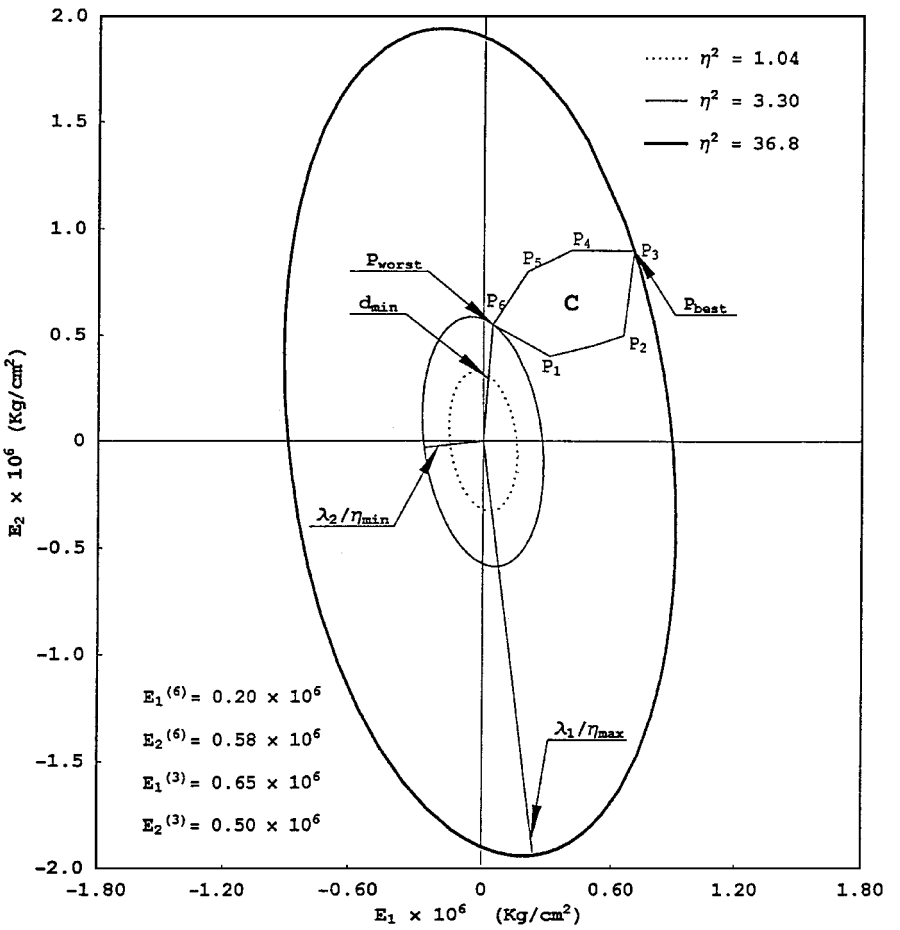

Fig. 2b Polygonal region of uncertainty with particular location of vertices P_3 and P_6.

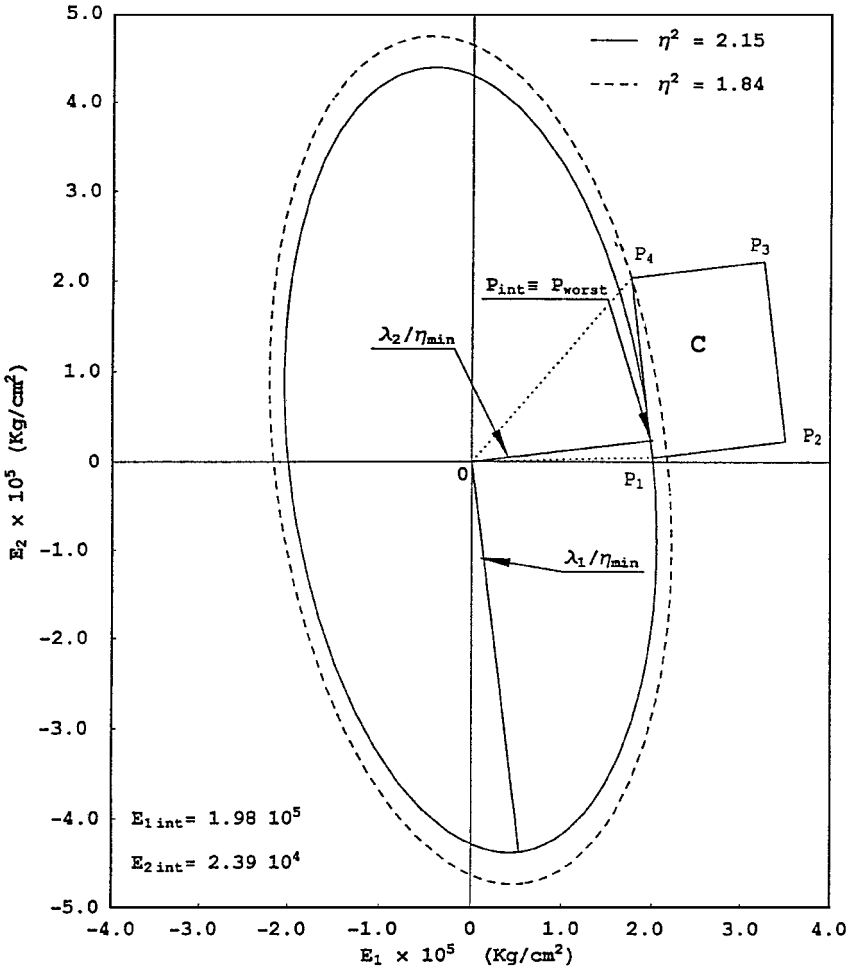

Fig. 2c Singular location for rectangular region of uncertainty; extrema noncoinciding with one of the vertices.

of the worst and best critical velocity $U^2_{\text{cr,worst}}$, and $U^2_{\text{cr,best}}$ are given by

$$U^2_{\text{cr,worst}} = \left(d_{11n}\bar{e}^2_{1,w} + 2d_{12n}\bar{e}_{1,w}\bar{e}_{2,w} + d_{22n}\bar{e}^2_{2,w}\right)b_0^2h_0^6$$

$$U^2_{\text{cr,best}} = \left(d_{11n}\bar{e}^2_{1,b} + 2d_{12n}\bar{e}_{1,b}\bar{e}_{2,b} + d_{22n}\bar{e}^2_{2,b}\right)b_0^2h_0^6 \qquad (42)$$

The obtained solution for the antioptimized critical flutter velocity $U^2_{\text{cr,worst}}$ shall be utilized to get the best possible value of a certain objective function involving it. The optimization of the antioptimized critical velocity is nothing other than looking for the best in the worst circumstances.

VII. Minimum Weight Design: Optimization Procedure

The optimal design process involves the beam's weight W

$$W = \rho b_0 h_0 \int_0^L \chi_b(x)\chi_h(x)\,\mathrm{d}x \qquad (43)$$

which is a monotonic function of the design variables, namely, the width b_0 and then depth h_0, at $x = 0$. The functions $\chi_b(x)$ and $\chi_h(x)$ governing the shape of the beam's cross section have been introduced in Eq. (2). Although b_0 and h_0 appear symmetrically in Eq. (43), the critical velocity is not a symmetric function of those variables.

We are interested in designing the system (i.e., determining the values of b_0 and h_0) that minimizes the mass of Eq. (43) in conjunction with the constraint on the critical flutter velocity U^2_{cr} whose value must be greater than a specified velocity U_0

$$U_{\text{cr}}(b_0, h_0) \geq U_0 \qquad (44)$$

Because U_{cr} is an interval variable $[U_{\text{cr,worst}}, U_{\text{cr,best}}]$, fulfillment of the inequality

$$U_{\text{cr,worst}}(b_0, h_0) \geq U_0 \qquad (45)$$

automatically leads Eq. (44) to be satisfied. Hereinafter we will deal with Eq. (45). It is rewritten in a form that is more appropriate to the design by utilizing the representation in Eq. (38). This yields

$$U_{\text{cr,worst}} = \eta^2_{\min} b_0 h_0^3 \geq U_0 \qquad (46)$$

where $\eta_{\min}$ is defined in Eq. (39). Let the manufacturing requirements demand that the values b_0 and h_0 vary in a box Γ:

$$b_{0l} \leq b_0 \leq b_{0u}, \qquad h_{0l} \leq h_0 \leq h_{0u} \qquad (47)$$

where b_{0l}, b_{0u} and h_{0l}, h_{0u} denote the boundary limits for the width and the thickness amplitudes, respectively. An additional constraint involving the design parameters b_0 and h_0 is concerned with the range of validity of the utilized mechanical theory. Because we apply the Bernoulli–Euler's theory, we specify an additional constraint over the design variables as follows:

$$b_0 \leq z h_0 \qquad (48)$$

Specifically, for the sake of determinacy z is fixed at 10. The optimization problem is then stated as follows:

$$\underset{b_0, h_0 \in}{\text{minimize}} \qquad W(b_0, h_0) \qquad (49a)$$

$$\text{subject to} \qquad g_1(b_0, h_0) = \eta_{\min} b_0 h_0^3 - U_0 \geq 0 \qquad (49b)$$

$$\text{subject to} \qquad g_2(b_0, h_0) = 10h_0 - b_0 \geq 0 \qquad (49c)$$

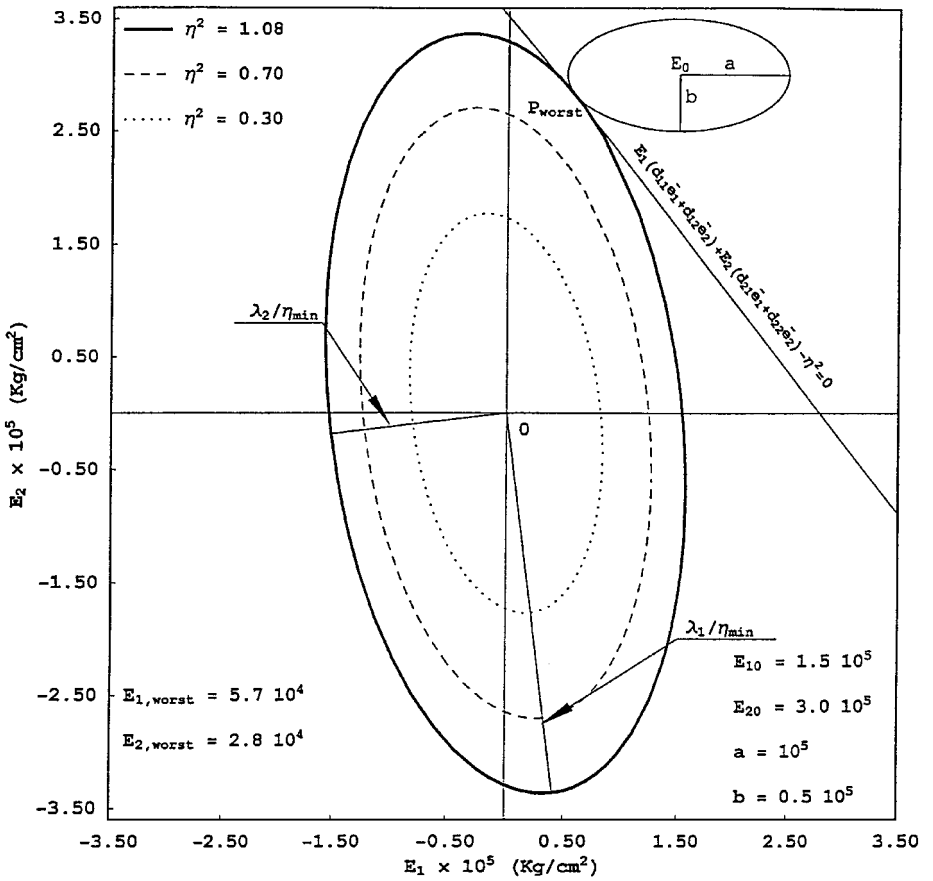

Fig. 3a Elliptical region of uncertainty; η^2_{min} ellipse.

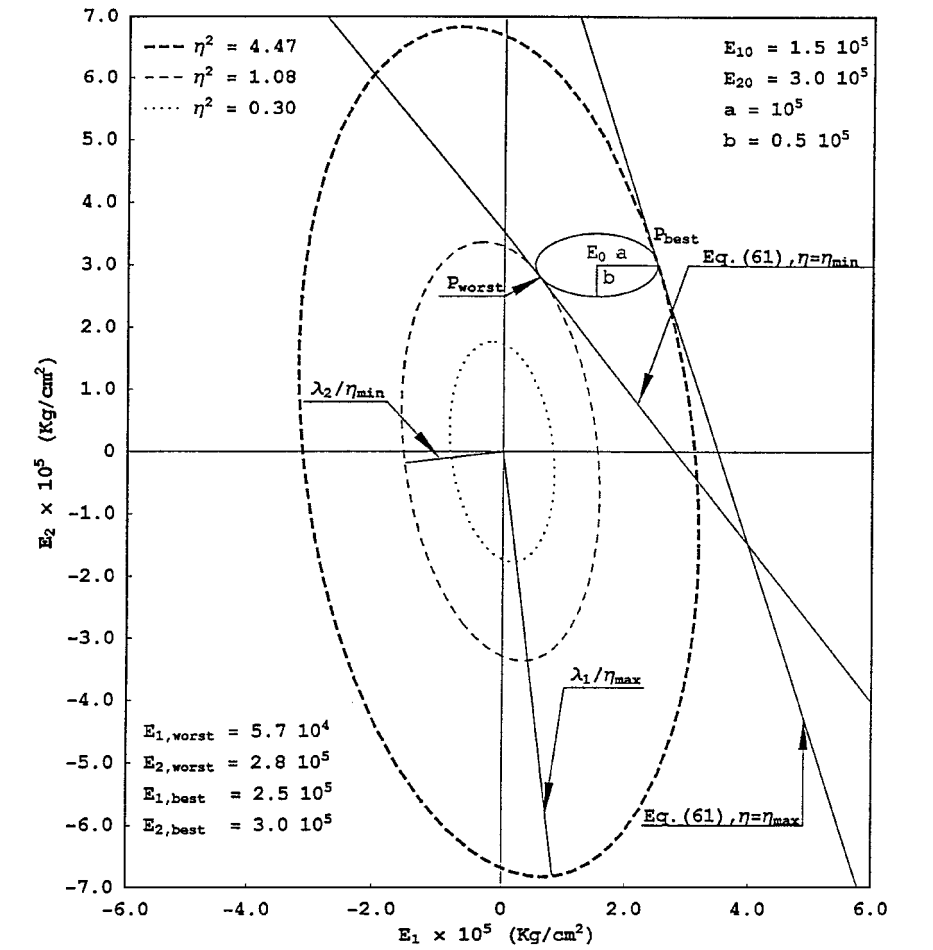

Fig. 3b Elliptical region of uncertainty; ellipses corresponding to the extrema values of the coefficient η^2.

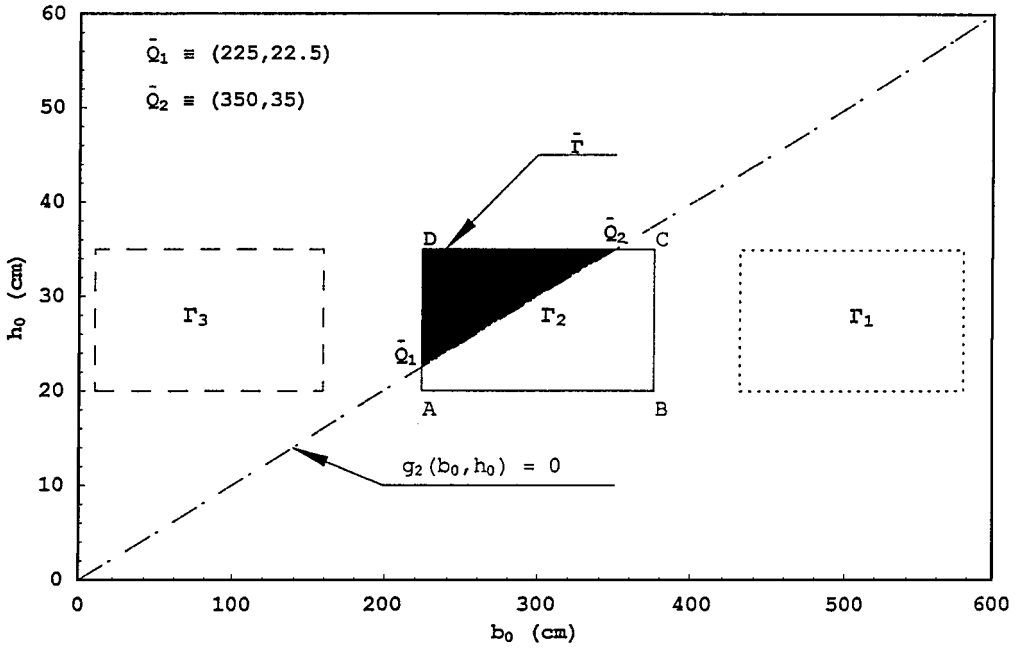

Fig. 4 Alternative locations of the design box with respect to the constraint $g_1 = 0$.

The optimization problem in Eq. (49) will be solved by employing geometrical considerations. Note that if in Eq. (48) the entire region of variation is on the right side of the line $g_2(b_0, h_0) = 0$, then no acceptable solution exists. In Fig. 4 this case is represented by the design region of variation drawn with a dotted line and denoted as Γ_1. If, however, the aforementioned line is positioned on the left side of the region in Eq. (48), the entire variation domain is feasible (see domain Γ_3 in Fig. 4). If the line $g_2(b_0, h_0) = 0$ passes through the region, only the upper part (see the hatched part of the area Γ_2 in Fig. 4) is a feasible domain. This particular location is portrayed in Fig. 4 as a continuous line. We denote by Q_1 and Q_2, respectively, the intersection points of the line $g_2(b_0, h_0) = 0$ with the region Γ that are closest and farthest from the origin O. Depending on the location of the region Γ with respect to the origin, several possibilities arise. If the line $g_2(b_0, h_0) = 0$ crosses the edges AD and CD, the intersection points have the coordinates

$$Q_1 \equiv (b_{0L}, 1/10b_{0L}), \qquad Q_2 \equiv (10h_{0u}, h_{0U}) \tag{50}$$

as shown in Fig. 4. Other possibilities of crossing the region by the line $g_2 = 0$ are elucidated in Figs. 5a–5c, where the coordinates of the intersection points are also indicated. To obtain the solution of the optimization problem in Eq. (49), let us examine closely the critical velocity constraint $g_1(b_0, h_0) \geq 0$. If the curve defined by

$$g_1(b_0, h_0) = \eta_{\min} b_0 h_0^3 - U_0 = 0 \tag{51}$$

lies below the feasible region $\bar{\Gamma}$, then the constraint [Eqs. (49b) and (49c)] is not active for the specified value of the velocity U_0. In this case the solution of the optimization coincides with the closest vertex of the hatched region $\bar{\Gamma}$ to the origin O. This vertex, denoted hereinafter $\bar{Q}_{\text{opt}}$, is either the point $\bar{Q}_1$, Figs. 4 and 5b, or A, Figs. 5a and 5c, respectively, if the straight line $g_2(b_0, h_0) = 0$ intersect the edge AD or AB. However, if the line in Eq. (46) is entirely above the hatched region $\bar{\Gamma}$, then no solution of the optimization problem exists for the specified value of the velocity U_0. Thus, we identify an interval $[U_{0,\min}, U_{0,\max}]$ where the specified velocity U_0 must lie so that the inequality $U_{\text{cr,worst}} \geq U_0$ may hold. The extreme values $U_{0,\min}$ and $U_{0,\max}$ of the admissible range of U_0 are given by

$$U_{0,\min} = \eta_{\min} b_{01} h_{01}^3 \tag{52a}$$

$$U_{0,\max} = \eta_{\min} b_{02} h_{02}^3 \tag{52b}$$

where the values b_{0i} and h_{0i} denote, respectively, the points in the feasible domain $\bar{\Gamma}$ with smallest and largest distances from the origin O, as represented in Figs. 6a and 6b. In Fig. 6a such extremal points are A and C, corresponding to $U_{0,\min} = 1.75 \times 10^7$ and $U_{0,\max} = 3.65 \times 10^8$. Hereinafter we assume that the specified velocity belongs to the following region $U_0 \in [U_{0\min}, U_{0\max}]$. Denote by $\tilde{\Gamma} \subseteq \bar{\Gamma}$ a region that is both feasible and satisfies the constraint on the critical velocity $U_{\text{cr,worst}}$ in Eq. (40). The weight in Eq. (43) is a monotonically increasing function in the variables b_0 and h_0. Therefore, the solution of the optimization problem lies on the boundary of the region $\tilde{\Gamma}$ closest to origin O. Moreover, we conclude that the solution of the optimization problem, denoted $Q_{\text{opt}} \equiv (b_{0,\text{opt}}, h_{0\text{opt}})$, coincides with the closest point to the origin O on the boundary of $\tilde{\Gamma}$.

To obtain the point Q_{opt} on the boundary with minimum distance OQ, we again resort to a geometric argument. Note that there exists a specific value of the distance OQ such that the family of circles (denoted by the dotted line in Figs. 6a and 6b)

$$b_0^2 + h_0^2 = OQ^2 \tag{53}$$

and the curve $g_1(b_0, h_0) = 0$ share a single point, that is, they have a common tangent in point $\bar{Q}(\bar{b}_0, \bar{h}_0)$ (Figs. 6a and 6b). The tangent line to the curve $g_1(b_0, h_0) = 0$ in a plane Ob_0h_0 passing through the point $\bar{Q} \equiv (\bar{b}_0, \bar{h}_0)$ reads

$$h_0 - \bar{h}_0 = \left.\frac{\mathrm{d}h_0}{\mathrm{d}b_0}\right|_{\substack{h_0=\bar{h}_0 \\ b_0=\bar{b}_0}} (b_0 - \bar{b}_0) = -\frac{\eta_{\min}\bar{h}_0^4}{3U_0}(b_0 - \bar{b}_0) \tag{54}$$

where

$$\frac{\mathrm{d}h_0}{\mathrm{d}b_0} = \left(\frac{\mathrm{d}b_0}{\mathrm{d}h_0}\right)^{-1} = \left(\frac{\mathrm{d}}{\mathrm{d}h_0}\left(\frac{U_0}{\eta_{\min}h_0^3}\right)\right)^{-1} = \left(-\frac{3U_0}{\eta_{\min}h_0^4}\right)^{-1} \tag{55}$$

The tangent to the circle in Eq. (53) is represented by

$$b_0\bar{b}_0 + h_0\bar{h}_0 - OQ^2 = 0 \tag{56}$$

In point $\bar{Q}$ the two straight lines in Eqs. (54) and (55) coincide. We conclude that the coefficients of the variables b_0 and h_0 in Eqs. (54) and (55) must be proportional, with proportionality constant denoted θ:

$$\bar{b}_0 = \theta\eta_{\min}\bar{h}_0^4 \tag{57a}$$

$$\bar{h}_0 = 3\theta U_0 \tag{57b}$$

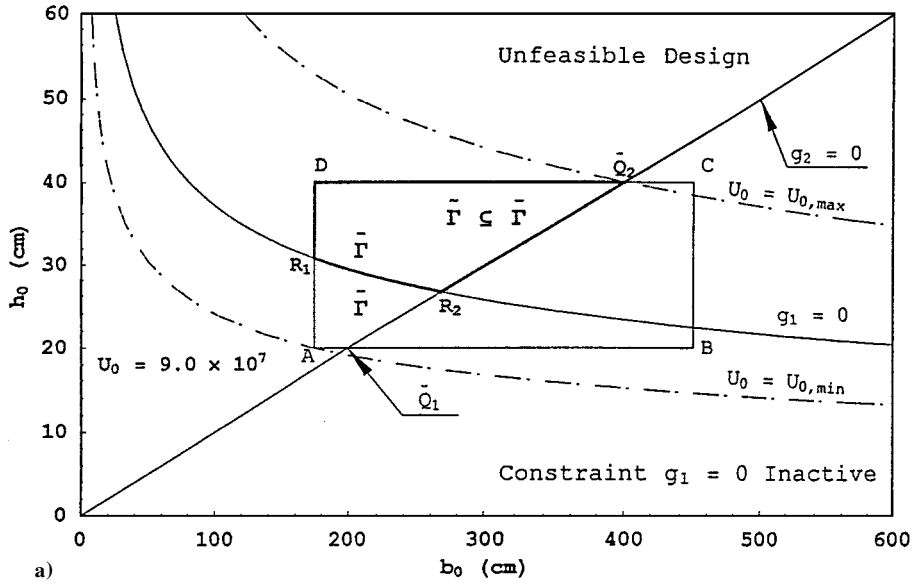

a)

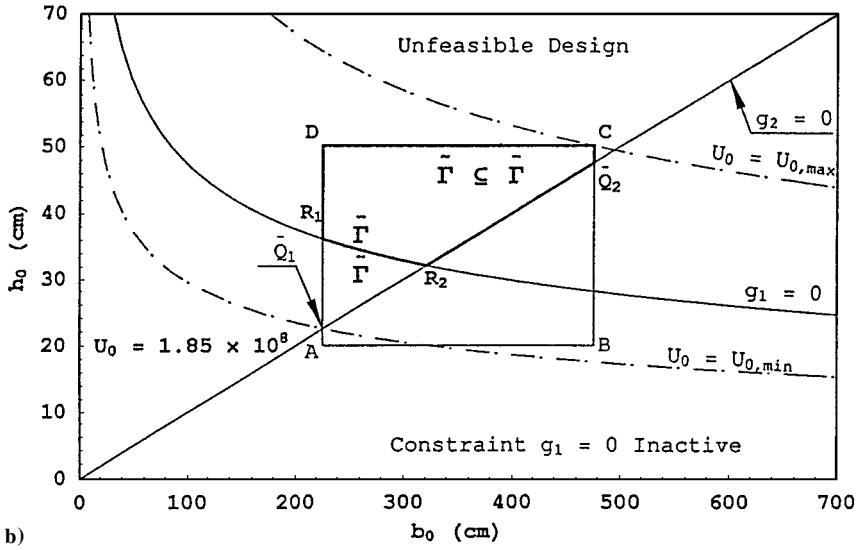

b)

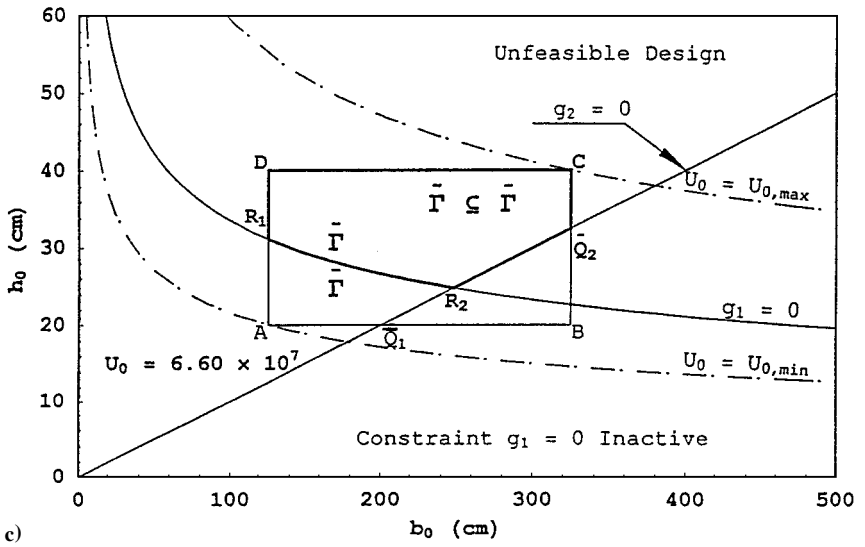

c)

Fig. 5 a) Feasible design region $\tilde{\Gamma}$ for specified velocity U_0. b) and c) Alternative locations of the design box with respect to constraints $g_1 = 0$ and $g_2 = 0$ for specified velocity U_0.

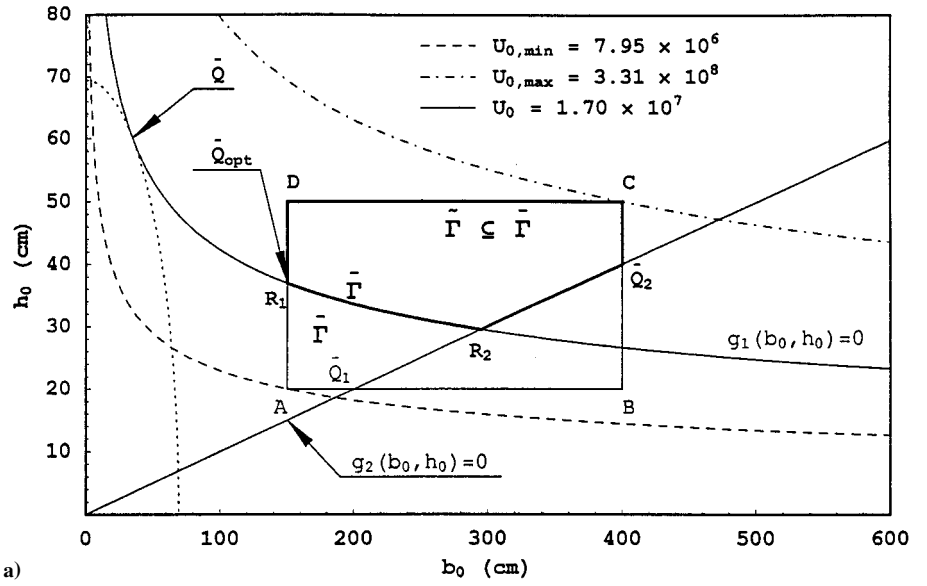

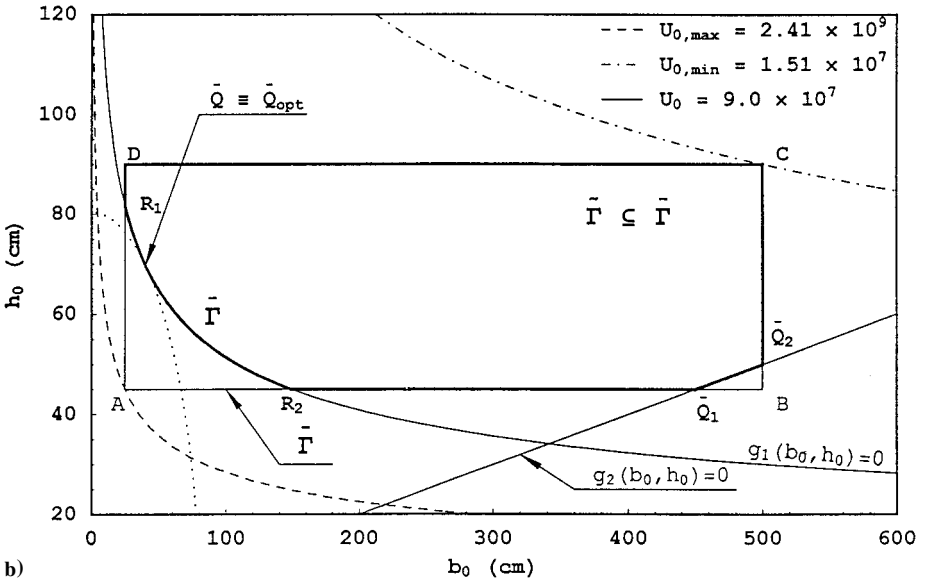

Fig. 6 Solution of the optimization problem a) on the closest vertex of the region $\tilde{\Gamma}$ and b) in correspondence of point $\bar{Q}$ in Eqs. (96) and (97).

The solution reads

$$\theta = \bar{h}_0/3\eta_{\min}, \qquad \bar{b}_0 = \bar{h}_0^5\eta_{\min}/3U_0 \tag{58}$$

We substitute $\bar{b}_0$ into Eq. (52a) to get $\bar{h}_0$:

$$\bar{h}_0 = \left(\sqrt{3U_0}\,|\,\eta_{\min}\right)^{\frac{1}{4}} \tag{59}$$

The value of $\bar{b}_0$ is found by substituting Eq. (59) and the expression for θ in Eq. (58) in the former Eq. (57a), getting

$$\bar{b}_0 = (3U_0/\eta_{\min})^{\frac{1}{4}} \tag{60}$$

We denote by R_1 and R_2, respectively, the intersection points of the curve $g_1(b_0, h_0) = 0$ with the boundaries of the region $\bar{\Gamma}$. If the point $\bar{Q}$ with coordinates $\bar{b}_0$, $\bar{h}_0$, defined in Eqs. (59) and (60), lies on the boundary of the feasible region (Fig. 6b) [i.e., is located on the arc R_1R_2 of the curve $g_1(b_0, h_0) = 0$], then the values of $\bar{b}_0$ and $\bar{h}_0$ so obtained represent the solution of the optimization problem in Eq. (49). If, however, the point $\bar{Q}$ is outside the admissible region (Fig. 6a), then the solution of the optimization problem is given by the vertex of the region $\bar{\Gamma}$ closest to the origin O.

VIII. Numerical Example

In this section we apply the present hybrid optimization and anti-optimization procedure to the optimal weight design of a simply supported beam. The length L of the beam will be assumed $L = 15$ m. The functions $\varphi_i(x)$ in Eq. (1) governing the variation of the modulus of elasticity E along the axis of the beam are chosen in the form

$$\varphi_1(x) = 1 + \sigma_1(x/L)^2 + \sigma_3(x/L)^4, \qquad \varphi_2(x) = \sigma_2(x/L)^5 \tag{61}$$

where the coefficients $\sigma_i (i = 1, 2, 3)$ represent some coefficients necessary to model the variation of the elastic modulus $E(x)$ along the axis of the beam. In the following the coefficients σ_i are set at $\sigma_1 = 1.1$, $\sigma_2 = 5.4$, and $\sigma_3 = 2.2$. The shape functions $\chi_b(x)$ and $\chi_h(x)$ in Eq. (2) governing, respectively, the geometric shape of the width $b(x)$ and of the height $h(x)$ are

$$b(x) = 1 + \varepsilon_1(x/L), \qquad h(x) = \left[1 + \varepsilon_2(x/L)^2\right] \tag{62}$$

where the coefficients ε_i, $i = 1, 2$, are introduced to control the variation of the cross section along the axis. Their values are fixed at

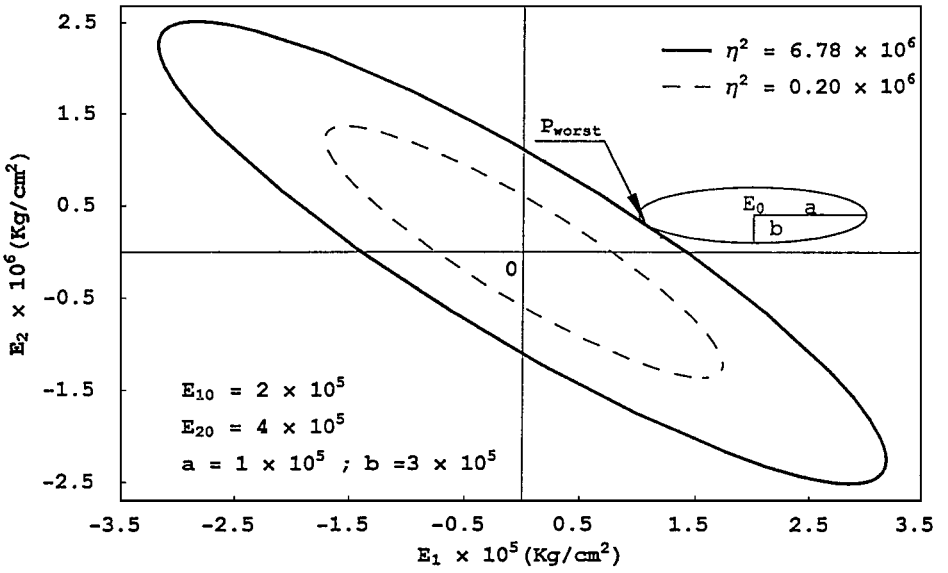

a) Determination of the minimum coefficient $\eta^2_{\min}$

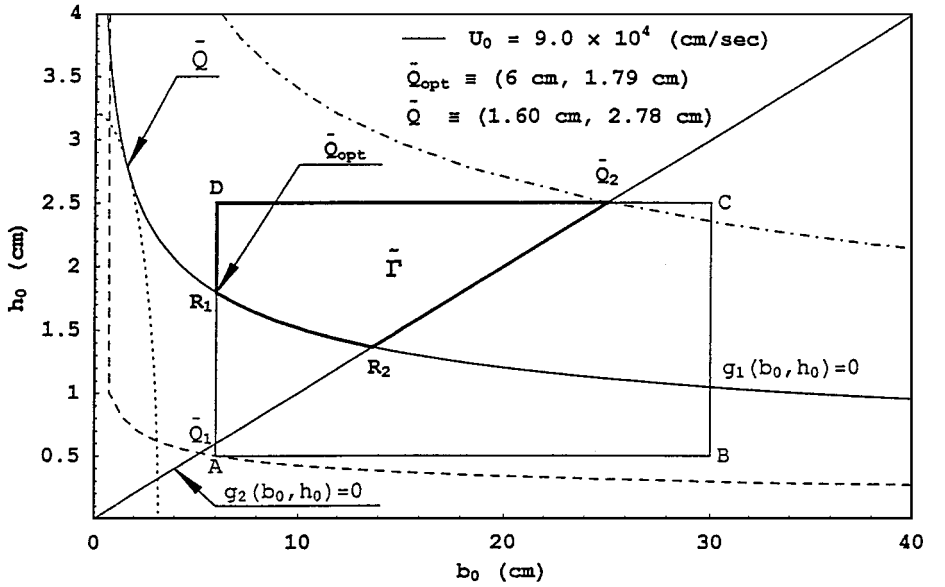

b) Solution of the design problem

Fig. 7 Application of the hybrid optimization and antioptimization.

$\varepsilon_1 = -0.7$ and $\varepsilon_2 = -0.73$. The uncertain coefficients E_1 and E_2, in Eq. (2) are assumed to vary in an ellipsoidal region. The coordinates E_{10} and E_{20} of the center and the semi-axes a and b of the ellipse are listed in Fig. 7a. The density of the structural material constituting the beam is set at $\rho = 2.7 \times 10^{-6}$ kg s^2/cm^4, whereas the aeroelastic parameters in Eq. (10) are $c_\infty = 3.3 \times 10^4$ cm/s and $k = 1.66$. The values of the coefficients d_{ijn} are $d_{11N} = 3.4 \times 10^{-5}$, $d_{12N} = 3.91 \times 10^{-6}$, and $d_{22N} = 5.5 \times 10^{-6}$, which yield a family of concentric ellipses after substituting the values of the coefficients d_{ijn} into Eq. (38). The generic ellipse of the family is represented by the dotted line in Fig. 7a. Equation (43), used to determine the coordinate $\bar{e}_1$ and $\bar{e}_2$, becomes

$$\gamma^4 - 7.81 \times 10^6 \gamma^3 - 6.32 \times 10^{13} \gamma^2 + 1.11 \times 10^{11} \gamma - 5.22 \times 10^{23} = 0 \tag{63}$$

whose lowest solution is to $\gamma = -5.07 \times 10^6$. The values of the abscissa and ordinate, respectively, of $\bar{e}_1$ and $\bar{e}_2$, are then $\bar{e}_1 = 1.06 \times 10^5$ and $\bar{e}_2 = 2.98 \times 10^5$. In Fig. 7a, the ellipse corresponding to the minimum η^2 and the tangent to the region of uncertainty in $P_w \equiv (\bar{e}_1, \bar{e}_2)$ is depicted with a continuous line. We assume that the design variables b_0 and h_0 assume values in the region

$$6\,\text{cm} \le b_0 \le 30\,\text{cm}, \qquad 0.5\,\text{cm} \le h_0 \le 2.5\,\text{cm} \tag{64}$$

represented in Fig. 7b. The lines corresponding to the extrema of the interval $[U_{0\min}, U_{0,\max}]$ are depicted, respectively, with dashed and dot–dashed line. The interval where the constraint $g_1(b_0, h_0) \ge 0$ is active is represented by $[1.9 \times 10^3, 1.02 \times 10^6]$. We set $U_0 =$ 900 m/s.

The region $\tilde{\Gamma}$ of variation of the design variables b_0 and h_0 is depicted by the area in Fig. 7b bounded by bold lines. The values of $\bar{b}_0$ and $\bar{h}_0$ corresponding to Eqs. (59) and (60) are listed in Fig. 7b. It is seen that they not belong to the boundary of the region $\tilde{\Gamma}$ as shown in Fig. 7b. Therefore, the combination of the design values b_0 and h_0 corresponding to a minimum of the weight $W(b_0, h_0)$ is found in the point $\bar{Q}_{\text{opt}}$ of coordinate $\bar{Q}_{\text{opt}} \equiv$ (6.0 cm, 1.79 cm). With the obtained values the minimum weight in this simple model is $W =$ 38.7 kg, which is the lowest value satisfying all of the constrains imposed on the system.

IX. Conclusions

In this study we discuss the flutter of a beam with uncertain modulus of elasticity that is simply supported at both ends, in a stream of

gas flow. The structural model has a variable cross section and variable modulus of elasticity along the axis of the beam to reflect the realistic situation. In this study we address the following question: How can the optimization methods in the presence of the bounded uncertainty that is neither probabilistic nor fuzzy, be utilized? The parameters describing the modulus of elasticity and were modeled as convex variables, belonging, respectively, to a polygonal hull of experimental points, or to an elliptic region. Combined optimization and antioptimization proved to be an effective tool for dealing with optimum design in the presence of uncertainty. The problem handled allowed us to elucidate the combined antioptimization procedure. We solved, at first, the problem to find an expression for the worst possible combination of the uncertain parameters involved in one of the constraints of the design variables. As a second step we optimized the design variables under the antioptimized version of one of the constraints.

Appendix A: Mutual Orientation of the Ellipses

To determine the orientation of the ellipse in Eq. (31) with respect of the region of variation of E_1 and E_2, we first find its semi-axes s_1 and s_2 by referring it to a rotated coordinate system (E_1', E_2') in which Eq. (31) of the conic is represented in its canonical form. The equation for the rotation of coordinates reads

$$E = \alpha^T E' \tag{A1}$$

where α denotes the transformation matrix and the vector E' is the coordinate vector in the rotated system with components E_1' and E_2'. Substitution into Eq. (31) yields

$$U_{\rm cr}^2 = E'^T \alpha D \alpha^T E' \tag{A2}$$

To get the equation of the ellipse in Eq. (A2) in the canonical form, we require the matrix $\alpha D \alpha^T$, in the following denoted as Λ, to be diagonal

$$\alpha D \alpha^T = \Lambda = \begin{pmatrix} \lambda_1 & 0 \\ 0 & \lambda_2 \end{pmatrix} \tag{A3}$$

where λ_i $(i = 1, 2)$ represent the sought diagonal terms. Equation (A3) is equivalent to the two scalar equations

$$\alpha_1 D \alpha_1^T = \lambda_1 \tag{A4}$$

$$\alpha_2 D \alpha_2^T = \lambda_2 \tag{A5}$$

Postmultiplying Eq. (A4) by α_1 and Eq. (A5) by α_2, and taking into account that $\alpha_i^T \alpha_i = 1$ $(i = 1, 2)$, we obtain

$$\alpha_1 (D - \lambda_1 I) = 0, \qquad \alpha_2 (D - \lambda_2 I) = 0 \tag{A6}$$

where I is an identity matrix. Equation (A6) shows that the axes of the new coordinate system $(E_1' \; E_2')$ of unit vectors α_1 and α_2 lie along the eigenvectors of the matrix D. The appropriate eigenvalue problem reads

$$\det |D - \lambda I| = 0 \tag{A7}$$

with the eigenvalues λ_i associated with the eigenvectors α_i.

Solution of Eq. (A7) furnishes the expression of the eigenvalues λ_i $(i = 1, 2)$

$$\lambda_{1,2} = (d_{11} + d_{22})/2 \pm \sqrt{(d_{11} - d_{22})^2 |\, 4 + d_{12}^2} \tag{A8}$$

where the minus sign is associated with λ_1 and the plus sign indicates λ_2. The components of the eigenvectors α_{ix} and α_{iy} read

$$\alpha_{1x} = \frac{-d_{12}}{\sqrt{(d_{11} - \lambda_1)^2 + d_{12}^2}}, \qquad \alpha_{1y} = \frac{(d_{11} - \lambda_1)}{\sqrt{(d_{11} - \lambda_1)^2 + d_{12}^2}}$$

$$\alpha_{2x} = \frac{-d_{12}}{\sqrt{(d_{11} - \lambda_2)^2 + d_{12}^2}}, \qquad \alpha_{2y} = \frac{(d_{11} - \lambda_2)}{\sqrt{(d_{11} - \lambda_2)^2 + d_{12}^2}} \tag{A9}$$

Equation (A2) in the new coordinate system (E_1', E_2') is cast as

$$U_{\rm cr}^2 = E'^T \Lambda E' \tag{A10}$$

or, in the canonical form,

$$\frac{\lambda_1 (E_1')^2}{U_{\rm cr}^2} + \frac{\lambda_2 (E_2')^2}{U_{\rm cr}^2} = 1 \tag{A11}$$

Equation (46) indicates that the semi-axes s_1 and s_2 of the ellipse are given by

$$s_1^2 = U_{\rm cr}^2 |\, \lambda_1, \qquad s_2^2 = U_{\rm cr}^2 |\, \lambda_2 \tag{A12}$$

From Eqs. (A8) and (A12) we conclude that $s_1 > s_2$. To determine the orientation of the ellipse in Eq. (A11) [i.e., directions of its major and minor axes in the plane (E_1, E_2)], we need to investigate the signs of the components of the eigenvectors α_1 and α_2 in Eq. (A9). After substitution of Eq. (A8) in Eq. (A9), we observe that the term $d_{11} - \lambda_1$ is positive whereas the term $d_{11} - \lambda_2$ is negative. In other words, $\alpha_{1y} > 0$ and $\alpha_{2y} < 0$. Because α_{1x} and α_{2x} depend on the term d_{12}, we conclude that the orientation of the ellipse [Eq. (A11)] in the plane (E_1, E_2) is decided by the sign of the term d_{12}. For positive d_{12}, the major axis of the ellipse passes through the second and fourth quadrants of the plane, because $\alpha_{1x} < 0$ and $\alpha_{1y} < 0$. The minor axis passes through the first and third quadrants because both of its directional cosines α_{2x} and α_{2y} are negative. However, if d_{12} proves to be negative, then the major and minor axes are interchanged.

It appears unfeasible to determine the sign of d_{12} analytically, without its direct numerical evaluation. We will limit ourselves with obtaining a sufficient condition for the positiveness of the term d_{12} without its calculation and, moreover, without specifying the functions $\rho A(x)$, $I(x)$, and functions $\varphi_i(x)$ and $\psi_i(x)$. Let us first consider the coefficients K_{ijl} in Eq. (30). Integration by parts, and accounting for the homogeneous boundary conditions, yields

$$K_{ijl} = \int_0^L I(x) \varphi_l(x) \frac{{\rm d}^2 \psi_i}{{\rm d}x^2} \frac{{\rm d}^2 \psi_j}{{\rm d}x^2} \, {\rm d}x \tag{A13}$$

Using dummy variables, the products in Eq. (29) can be cast as double integrals:

$$M_{22} K_{111} = \int_0^L \rho A(x) \psi_2^2(x) \, {\rm d}x \int_0^L I(x) \varphi_1(x) \left(\frac{{\rm d}^2 \psi_1}{{\rm d}x^2} \right) {\rm d}x$$

$$= \int\int_{D_b} \rho A(\xi) \psi_2^2(\xi) I(x) \varphi_1(x) \left(\frac{{\rm d}^2 \psi_1}{{\rm d}x^2} \right) {\rm d}x \, {\rm d}\xi \tag{A14}$$

where D_b indicates the square $[0, L] \times [0, L]$. Analogously, the following quantities are represented as double integrals:

$$M_{11} K_{221} = \int\int_{D_b} \rho A(\xi) \psi_1^2(\xi) I(x) \varphi_1(x) \left(\frac{{\rm d}^2 \psi_2}{{\rm d}x^2} \right)^2 {\rm d}x \, {\rm d}\xi$$

$$M_{22} K_{112} = \int\int_{D_b} \rho A(\xi) \psi_2^2(\xi) I(x) \varphi_2(x) \left(\frac{{\rm d}^2 \psi_1}{{\rm d}x^2} \right)^2 {\rm d}x \, {\rm d}\xi$$

$$M_{11} K_{222} = \int\int_{D_b} \rho A(\xi) \psi_2^2(\xi) I(x) \varphi_2(x) \left(\frac{{\rm d}^2 \psi_2}{{\rm d}x^2} \right)^2 {\rm d}x \, {\rm d}\xi$$

$$M_{12} K_{211} = \int\int_{D_b} \rho A(\xi) \psi_1(\xi) \psi_2(\xi) I(x) \varphi_1(x) \frac{{\rm d}^2 \psi_1}{{\rm d}x^2} \frac{{\rm d}^2 \psi_2}{{\rm d}x^2} \, {\rm d}x \, {\rm d}\xi$$

$$M_{12} K_{212} = \int\int_{D_b} \rho A(\xi) \psi_1(\xi) \psi_2(\xi) I(x) \varphi_2(x) \frac{{\rm d}^2 \psi_1}{{\rm d}x^2} \frac{{\rm d}^2 \psi_2}{{\rm d}x^2} \, {\rm d}x \, {\rm d}\xi \tag{A15}$$

The terms δ_1 and δ_2 in Eq. (29) become

$$\delta_1 = \iint_{D_b} \rho A(\xi) I(x) \varphi_1(x) \times \left(\psi_2(\xi) \frac{\mathrm{d}^2 \psi_1(x)}{\mathrm{d}x^2} - \psi_1(\xi) \frac{\mathrm{d}^2 \psi_2(x)}{\mathrm{d}x^2} \right)^2 \mathrm{d}x\, \mathrm{d}\xi$$

$$\delta_2 = \iint_{D_b} \rho A(\xi) I(x) \varphi_2(x) \times \left(\psi_2(\xi) \frac{\mathrm{d}^2 \psi_1(x)}{\mathrm{d}x^2} - \psi_1(\xi) \frac{\mathrm{d}^2 \psi_2(x)}{\mathrm{d}x^2} \right)^2 \mathrm{d}x\, \mathrm{d}\xi \tag{A16}$$

because $M_{12} K_{211} = M_{21} K_{121}$. The coefficient ε_{12} in Eq. (29) assumes the following form:

$$\varepsilon_{12} = \iint_{Db} I(x) I(\xi) \varphi_1(x) \varphi_2(\xi) \times \left(\frac{\mathrm{d}^2 \psi_1}{\mathrm{d}x^2} \frac{\mathrm{d}^2 \psi_2}{\mathrm{d}\xi^2} - \frac{\mathrm{d}^2 \psi_2}{\mathrm{d}x^2} \frac{\mathrm{d}^2 \psi_1}{\mathrm{d}\xi^2} \right)^2 \mathrm{d}x\, \mathrm{d}\xi \tag{A17}$$

because $K_{121} = K_{211}$ and $K_{122} = K_{212}$. Equations (A16) and (A17) illustrate that the terms δ_j and ε_{12} are positive if the uncertain variation functions $\varphi_1(x)$ and $\varphi_2(x)$ are positive valued in the domain $[0, L]$. The term d_{12} in Eq. (32) is positive if the terms δ_j and ε_{12} satisfy the following condition:

$$\delta_1 \delta_2 \geq 2\varepsilon_{12} \det[M_{\alpha\beta}] \tag{A18}$$

Let us discuss first the auxiliary problem of a beam of the same geometry as the one under study, but with the modulus of elasticity specified as $E(x) = \varphi_1(x)$ or $E(x) = \varphi_2(x)$. Through Galerkin's method with two-term approximation, we express the natural frequency by means of Eq. (18), except that we replace the expression of K_{ij} with K_{ij1} or K_{ij2}, respectively. Bearing in mind Eq. (29) for ε_{11} and ε_{22}, we conclude that

$$\det[K_{ij1}] = \varepsilon, \qquad \det[K_{ij2}] = \varepsilon_{22} \tag{A19}$$

Both terms ε_{11} and ε_{22} are positive as the determinants of the stiffness matrices. Moreover, expression for c_2 in Eq. (28) is a positive-definite quadratic form because the term c_2 represents the product of the natural frequencies ω_1^2 and ω_2^2, as can be detected from Eq. (18). We conclude that the following inequality holds:

$$\sqrt{\varepsilon_{11} \varepsilon_{22}} \geq \varepsilon_{12} \tag{A20}$$

If $\varphi_1(x)$ and $\varphi_2(x)$ are positive-valued functions we can write the inequalities

$$\delta_1 \geq 2\sqrt{|M_{\alpha\beta}| \varepsilon_{11}}, \qquad \delta_2 \geq 2\sqrt{|M_{\alpha\beta}| \varepsilon_{22}} \tag{A21}$$

Moreover,

$$\delta_1 \delta_2 \geq 4|M_{\alpha\beta}| \sqrt{\varepsilon_{11} \varepsilon_{22}} \tag{A22}$$

With Eq. (A21) taken into account, the following inequalities are obtained:

$$\delta_1 \delta_2 \geq 4|M_{\alpha\beta}| \sqrt{\varepsilon_{11} \varepsilon_{22}} \geq 4|M_{\alpha\beta}| \varepsilon_{12} \geq 2|M_{\alpha\beta}| \varepsilon_{12} \tag{A23}$$

which concludes the proof that d_{12} is positive. Thus, the orientation of the ellipse in Eq. (31) is determined, with its major axis passing through the second and fourth quadrants.

Appendix B: Solution in Case of Polygonal Region of Uncertainty

Except for a special case that will be considered later, the point P_{worst} corresponding to the minimum ratio $\eta^2_{\min}$ is located on the vertex P_i of the polygon C with the minimum distance form the origin O. Thus, this point is identified through the relation

$$O P_{\min} = \min_{d_i \in V} d_i \tag{B1}$$

In Fig. 2a the uncertainty region C is represented by rectangular shape that has a generic orientation with respect to the axes E_1 and E_2. The ellipse corresponding to the extremal values $\eta^2_{\min}$ of the coefficient η^2 are shown in Fig. 4a by continuous curves. The vertex P_4 with the minimum distance from the coordinate origin O is identified as $P_{\min} \equiv P_{\text{worst}}$. The point with maximum distance from the origin O is identified as $P_{\max} \equiv P_{\text{best}}$. Note that although a rectangular region has been considered, the same solution is valid for any polygonal region of uncertainty if the vertex closest to the origin O coincides with the point P_4 and the farthest vertex coincides with point P_2 in Fig. 2a. This is illustrated in Fig. 2b, where instead of the rectangular region in Fig. 2b we have a generic hexagonal region of uncertainty. According to our convention on denoting the vertices, point P_6 in Fig. (2b) coincides with the location of point P_4 in Fig. 2a; moreover, the point P_3 in Fig. 2b coincides with the location of point P_2 in Fig. 2a. Yet, these two different cases yield the same results for the worst and the best critical velocities. The coordinates of point P_6 and P_3 are located in Fig. 2b. Let us consider a location of the region C as depicted in Fig. 2b. The convex hull C of the experimental points, represented by a rectangular domain, is located in such a specified manner that the direction identified by the minor axis of the ellipse is perpendicular to the edge closest to the origin of the coordinate system O. Let us consider a line that is an extension the minor axis as

$$E_2 = (\alpha_{2y}/\alpha_{2x}) E_1 = -[(d_{11} - \lambda_2)/d_{12}] E_2 \tag{B2}$$

with α_{2x} and α_{2y} represented in Eq. (36). The line passing through points P_1 and P_4 is given by

$$E_2 = \frac{(E_{2.4} - E_{2.1}) E_1 + E_{1.4} E_{2.1} - E_{2.4} E_{1.1}}{E_{1.4} - E_{1.1}} \tag{B3}$$

The point of intersection of the lines in Eqs. (B2) and (B3) is denoted as $P_{\text{int}} \equiv (E_{1,\text{int}}, E_{2,\text{int}})$. The abscissa $E_{1\,\min t}$ and the ordinate $E_{2,\text{int}}$ are found by solving the system formed by Eqs. (B2) and (B3). The solution of these two equations reads

$$E_{1,\text{int}} = \frac{d_{12}(E_{2.4} E_{1.1} - E_{1.4} E_{2.1})}{d_{12}(E_{2.4} - E_{2.1}) + (d_{11} - \lambda_2)(E_{1.4} - E_{1.1})}$$

$$E_{2,\text{int}} = \frac{(d_{11} - \lambda_2)(E_{2.4} E_{1.1} - E_{1.4} E_{2.1})}{d_{12}(E_{2.4} - E_{2.1}) + (d_{11} - \lambda_2)(E_{1.4} - E_{1.1})} \tag{B4}$$

The point P_{int} naturally corresponds to the worst critical velocity; hence, we denote it as $P_{\text{int}} \equiv P_{\text{worst}}$ (see Fig. 4b). We observe, from Fig. 4b, that the distances $O P_1$ and $O P_4$ are both greater than the distance $O P_{\text{int}}$ because $O P_1$ and $O P_4$ are hypotenuses of the right triangles $O P_1 P_{\text{int}}$ and $O P_4 P_{\text{int}}$, respectively. The solution of the antioptimization problem corresponding to minimum of the coefficient η^2 is obtained by substitution of the coordinates in Eq. (B4) into Eq. (38). The expression of the worst critical velocity $U^2_{\text{cr,worst}}$ is then furnished by substituting the expression η^2_{worst} into Eq. (37):

$$U^2_{\text{cr}} = \eta^2_{\min} b_0^2 h_0^6 = b_0^2 h_0^6 \left[d_{11n} (E_{1,\text{int}})^2 + 2 d_{12n} E_{1,\text{int}} E_{2,\text{int}} + d_{22n} (E_{2,\text{int}})^2 \right] \tag{B5}$$

It is remarkable that, up to now, no assumptions have been made about the functions $\varphi_1(x)$, $\varphi_2(x)$, $\xi_b(x)$, or $\xi_h(x)$. Therefore, Eqs. (39) and (B5) represent general expressions for the extrema of the critical velocity, when E_1 and E_2 are varying in the rectangular region C.

Appendix C: Solution in Case of Elliptic Region of Uncertainty

In the points P_{worst} and P_{best} the ellipses in Eqs. (39) and (41) must share a common tangent. This consideration is utilized to get the coordinates of the contact points. The tangent to the ellipse in Eq. (41) in a generic point $P \equiv (e_1, e_2)$ reads as follows:

$$\left[E_1(e_1 - E_{10}) - E_{10}e_1 + E_{10}^2\right] \mid a^2 + \left[E_2(e_2 - E_{20}) - E_{20}e_2 + E_{20}^2\right] \mid b^2 - 1 = 0 \tag{C1}$$

Therefore, the tangent to the ellipse in Eq. (39) is represented as

$$E_1(d_{11n}e_1 + d_{12n}e_2) + E_2(d_{22n}e_2 + d_{12n}e_1) - \eta^2 = 0 \tag{C2}$$

For the two lines in Eqs. (C1) and (C2) to coincide, it is necessary and sufficient that the coefficients in front of e_1 and e_2 be proportional, with the ratio denoted as γ,

$$\frac{a^2(d_{11n}e_1 + d_{12n}e_2)}{e_1 - E_{10}} = \frac{b^2(d_{22n}e_2 + d_{12n}e_1)}{e_2 - E_{20}} = \frac{\eta^2}{E_{10}e_1 \mid a^2 + E_{20}e_2 \mid b^2 - \left(E_{20}^2 \mid b^2 + E_{10}^2 \mid a^2 - 1\right)} \equiv \gamma \tag{C3}$$

These equations can be rewritten as

$$\begin{aligned} a^2(d_{11}e_1 + d_{12}e_2) &= \gamma(e_1 - E_{10}) \\ b^2(d_{22}e_2 + d_{12}e_1) &= \gamma(e_2 - E_{20}) \\ \eta^2 &= \gamma\left[E_{10}e_1 \mid a^2 + E_{20}e_2 \mid b^2 - \left(E_{20}^2 \mid b^2 + E_{10}^2 \mid a^2 - 1\right)\right] \end{aligned} \tag{C4}$$

yielding an algebraic system of three equations, in four unknowns e_1, e_2, η^2, and γ. An additional condition to be imposed is that the solution must belong to the boundary of the uncertainty region C. The solution of the former two equations, hereinafter denoted as $\bar{e}_1(\gamma)$ and $\bar{e}_2(\gamma)$, is given by

$$\begin{aligned} \bar{e}_1 &= \frac{\gamma\left(E_{10}\gamma + a^2 d_{12n}E_{20} - b^2 d_{22n}E_{10}\right)}{\gamma^2 - \left(a^2 d_{11n} + b^2 d_{22n}\right)\gamma + a^2 b^2 D_n} \\ \bar{e}_2 &= \frac{\gamma\left(E_{20}\gamma + b^2 d_{12n}E_{10} - a^2 d_{11n}E_{20}\right)}{\gamma^2 - \left(a^2 d_{11n} + b^2 d_{22n}\right)\gamma + a^2 b^2 D_n} \end{aligned} \tag{C5}$$

where D_n represents the following determinant:

$$D_n = \begin{vmatrix} d_{11n} & d_{12n} \\ d_{12n} & d_{22n} \end{vmatrix} \tag{C6}$$

The parameter γ is determined by imposing the condition that the point in Eq. (C5) belongs to the boundary of the elliptic in Eq. (C1). We substitute Eq. (C5) into Eq. (C.1) yielding the following fourth order polynomial equation in terms of γ:

$$f(\gamma) = \gamma^4 - 2q_1\gamma^3 + q_2\gamma^2 - q_3\gamma + q_4 = 0 \tag{C7}$$

with the coefficients

$$\begin{aligned} q_1 &= \left(a^2 d_{11n} + b^2 d_{22n}\right) \\ q_2 &= \left(a^2 d_{11n} + b^2 d_{22n}\right)^2 + a^2 b^2 D_n - a^4(d_{11n}E_{10} + d_{12n}E_{20})^2 - b^4(d_{12n}E_{10} + d_{22n}E_{20})^2 \\ q_3 &= \left[\left(a^2 d_{11n} + b^2 d_{22n}\right)a^2 b^2 + (E_{10}d_{11n} + E_{20}d_{12n})a^4 b^2\right]D_n + b^4 a^2(d_{12n}E_{10} + d_{22n}E_{20})D_n \\ q_4 &= -a^4 b^4 D_n^2 \end{aligned} \tag{C8}$$

Once the solution of Eq. (C7) is obtained, the coordinates of the contact points' coordinates are finally determined via Eq. (C5). We need to investigate the roots of Eq. (C7). We first observe that coefficient q_4 in Eq. (C8) is negative because D_n is positive. Denoting the roots of the polynomial equation γ_j by means of Vieta's theorem we write

$$q_4 = \gamma_1\gamma_2\gamma_3\gamma_4 \tag{C9}$$

The negativity of q_4 assures that not all of the roots of the polynomial equation in Eq. (C7) are complex numbers. Indeed, if Eq. (C7) had four complex roots, then because they appear in complex conjugate pairs, their product in Eq. (C9) would be positive. However, because q_4 is negative the roots can appear as either four real roots, or two real and a complex conjugate pair, depending on the parameters of the system. If the polynomial equation in Eq. (C7) has two real and two complex conjugate roots then the substitution of the two real values of γ_i, ($i = 1, 2, 3,$ and 4) in Eq. (C7) will provide the coordinates of the contact P_{worst} and P_{best}. In case of four real roots corresponding to Eq. (C7), only two of them will correspond to tangency points of the ellipses in Eqs. (39) and (41).

Figure 3a portrays an example for the ellipse corresponding to the minimum coefficient η^2 while E_1 and E_2 vary in region C. The coordinates of the tangency point between the η^2 ellipse and the uncertainty C are listed in Fig. 3a. An illustrative representation of the region of variation of the uncertain parameters E_1 and E_2 and the ellipses corresponding to the maximum and the minimum value of η^2 are given in Fig. 3b. The ellipse corresponding to $\eta^2_{\min}$ is represented with dotted line, and the ellipse corresponding to $\eta^2_{\max}$ is depicted with dashed line. The ellipse representing the uncertainty region is drawn with continuous line. The tangents as well as the coordinates of P_{best} and P_{worst} are shown in Fig. 3b in conjunction with the values of the coefficients $\eta^2_{\min}$ and $\eta^2_{\max}$.

Acknowledgments

This study was conducted when M. Zingales served as Visiting Research Fellow in the Department of Mechanical Engineering of Florida Atlantic University under the financial support of the Italian Ministry of Technology and Scientific Research. The work of I. Elishakoff was supported by National Science Foundation Grant 99-10195 (K. P. Chong, Program Director).

References

[1]Elishakoff, I., "Convex Versus Probabilistic Modeling of Uncertainty in Structural Dynamics," *Structural Dynamics Recent Advances*, edited by M. Petyt, H. F. Wolfe, and C. Mei, Keynote Lecture, Elsevier, London, 1991, pp. 3–21.

[2]Elishakoff, I., "An Idea of the Uncertainty Triangle," *Shock and Vibration Digest*, Vol. 22, No. 10, 1990, pp. 1.

[3]Elishakoff, I., Haftka, R. T., and Fang, J., "Structural Design under Bounded Uncertainty-Optimization with Anti-Optimization," *Computers and Structures*, Vol. 53, No. 6, 1994, pp. 1401–1406.

[4]Adali, S., Elishakoff, I., Richter, A., and Verijenko, V. E., "Optimal Design of Symetric Angle-Ply Laminated for Maximum Buckling Load with Scatter in Material Properties," *5th AIAA/USAF/NASA/ISSMO Symposium on Multidisciplinary Analysys on Optimization*, AIAA, Washington DC, 1994, pp. 1041–1045.

[5]Haftka, R. T., and Lombardi, M., "Anti-Optimization Technique for Structural Design under Load Uncertainties," *Computer Methods in Applied Mechanics and Engineering*, Vol. 157, 1998, pp. 19–31.

[6]Turner, M. J., "Optimization of Structures to Satisfy Flutter Requirements," *AIAA Journal*, Vol. 7, No. 5, 1969, pp. 233–239.

[7]Plaut, R. H., "Structural Optimization of a Panel Flutter Problem," *AIAA Journal*, Vol. 9, No. 1, 1971, pp. 182–184.

[8]Ashley, H., "On Making Things the Best: Aeronautical Uses of Optimization," *Journal of Aircraft*, Vol. 19, No. 1, 1982, pp. 5–28.

[9]Librescu, L., and Bainer, L., "Aeroelastic Optimization of Orthotropic Rectangular Flat Panels," *Optimal Control Applications and Methods*, Vol. 4, 1983, pp. 193–198.

[10]Shirk, M. H., Hertz, T. H., and Weisshaar, T. A., "Aeroelastic Tailoring: Theory, Practice, and Promise," *Journal of Aircraft*, Vol. 23, No. 1, 1986, pp. 6–18.

[11]Ringertz, U. T., "On Structural Optimization with Aeroelastic Constraints," *Structural Optimization*, Vol. 8, 1994, pp. 16–23.

[12]Livne, E., and Mineau, D., "Panel Flutter Constraints: Analytic Sensitivities and Approximations Including Planform Shape Design Variables," *Journal of Aircraft*, Vol. 34, 1997, pp. 558–568.

[13]Pierson, B. L., and Genalo, L. J., "Minimum Weight Design of a Rectangular Panel Subjected to a Flutter Speed Constraint," *Computer Methods in Applied Mechanics and Engineering*, Vol. 10, 1977, pp. 45–62.

[14]Bishop, J. A., Eastep, F. E., Striz, A. G., and Venkayya, V. B., "Influence of Model Complexity and Aeroelastic Constraints on Multidisciplinary Optimization of Wings," *Journal of Aircraft*, Vol. 35, 1998, pp. 784–790.

[15]Kuttekeuler, J., and Ringertz, U., "Aeroelastic Tailoring Considering Uncertainties in Material Properties," *Structural Optimization*, Vol. 15, 1998, pp. 157–162.

[16]Liaw, D. G., and Yang, T. Y., "Reliability of Initially Compressed Uncertain Laminated Plates in Supersonic Flow," *AIAA Journal*, Vol. 29, No. 1, 1990, pp. 52–60.

[17]Shinozuka, M., "Structural Response Variability," *Journal of Engineering Mechanics*, Vol. 113, 1987, pp. 825–842.

[18]Livne, E., "Integrated Areoservoelastic Optimization: Status and Direction," AIAA Paper 97-1409, 1997.

[19]Ben-Haim, Y., and Elishakoff, I., "Geometric Imperfections" *Convex Models of Uncertainty in Applied Mechanics*, Elsevier, Amsterdam, 1990, pp. 135–151.

[20]Ashley, H., and Zartarian, C., "Piston Theory—A New Aerodynamic Tool for the Aeroelastician," *Journal of the Aeronautical Sciences*, Vol. 23, 1956, pp. 1109–1118.

[21]Il'yushin, A. A., "The Law of Plane Sections at High Supersonic Velocities," *PPM–Journal of Applied Mathematics and Mechanics*, Vol. 20, 1956 (in Russian).

[22]Bolotin, V. V., "Stability of Elastic Bodies in a Gas Flow," *Non-Conservative Problems in the Theory of Elastic Stability*, Pergamon, New York, 1963, pp. 242–257.

[23]Panovko, Ya. G., and Gubanova, I. I., *Stability and Oscillations of Elastic Systems, Paradoxes, Fallacies and New-Concepts*, Consultants Bureau, New York, 1965, pp. 215–231.

A. Messac
Associate Editor